Non-Photochemical Laser-Induced Nucleation in Supercooled Water

Emilia Sörlén Hagrot
emilia.hagrot@gmail.com

under the direction of
M.Sc. Niloofar Esmaeildoost
Associate prof. Jonas Sellberg
Biomedical and X-Ray Physics
Department of Applied Physics
KTH Royal Institute of Technology

Research Academy for Young Scientists
July 14, 2021

Abstract

Non-photochemical laser-induced nucleation (NPLIN) in supercooled water is a moderately new method that was introduced in the mid 90s allowing to finely control nucleation both spatially and temporally. This control initiates a possibility to investigate how water nucleates to form ice as a fundamental part of natural frequent processes and for instance in research regarding climate change and pharmaceutical production. The aim of this study was therefore to determine the lower threshold of power for laser induction. Liquid droplets were hit by a laser and compared to spontaneous nucleation through calculations of conditions as well as error estimation using Monte Carlo simulations. In conclusion, boundaries of the threshold was, despite not determining the specific lower threshold or inducing the nucleation, identified as a power of 10 W, which is applicable for further research.

Acknowledgements

I would like to express my gratitude towards M.Sc. Niloofar Esmaeildoost to her extent of invaluable expertise in this field and for peer reviewing this paper. Moreover, I would also like to thank my research colleague Viktor Kollberg for discussions and imperative support. Additionally Associate Prof. Jonas Sellberg generosity of premission to work in the laboratory at AlbaNova and for intriguing discussions. Max Kenning also contributed with vital support and exquisite coffee wind downs during the demanding period of writing this paper. Furthermore, my thanks goes out to organizers and X-rays peer reviewing this paper. I At last I thank Rays - For Excellence and their partners of collaboration Kjell & Märta Beijers Stiftelse as well as Olle Engkvists Stiftelse for this wonderful opportunity of participation in research.

Contents

1 Introduction

Climate change and pharmaceutical development pose two great challenges to humanity. The field of crystal nucleation is of fundamental interest as it occurs persistently in our natural environment and plays a vital role in the production of pharmaceutics as well as in climate change research. Nucleation is defined as the initial event of the formation of a new phase, for instance thermodynamic, from another. Particularly in atmospheric science, it is crucial to determine how liquid water nucleates into ice on a microscopic level since it has a significant impact on the properties of aerosol particles in clouds and therefore on the climate [1, 2]. Furthermore, pharmaceutical productions considers the crystallization as it influences the crystal polymorphic structure, specifically in order to minimize lattice energy [3].

1.1 Theoretical Background

A general description of crystal nucleation is essential in order to understand this study. This will be explained in a following subsection and subsequently the favoured method non-photochemical laser-induced nucleation (NPLIN). This is followed by complementary equations suitable for the study.

1.1.1 Crystal Nucleation

The classical nucleation theory (CNT), is an approximate theory of nucleation of a new thermodynamic phase. It was developed 90 years ago by Gibbs et al. [4]. This theory describes condensation and is particularly applied to crystallization of supercooled liquid as a solid cluster formed by aggregation. Equation (1) calculates ΔG_N which is the Gibbs free energy of a spherical crystalline of a spherical cluster of radius r containing water molecules, $4\pi r^2\gamma_S$ is the surface term and $\frac{4\pi}{3}r^3\Delta\mu_V$ is the volume term. That is in which γ_S describes the interaction between interfacial free energy and $\Delta\mu_V$ free energy difference between liquid and crystal. See diagram in Figure for illustration of the theory behind

the equation 1 [1, 3].

$$\Delta G_N = 4\pi r^2 \gamma_S - \frac{4\pi}{3} r^3 \Delta\mu_V \tag{1}$$

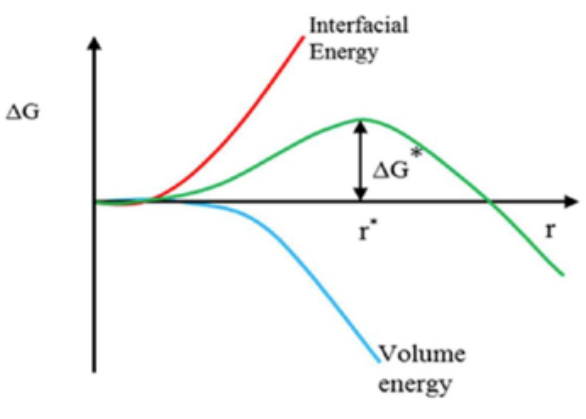

Figure 1: Diagram of free energy difference ΔG_N as a function of the crystalline nucleus radius.

Furthermore, there are two different classifications of nucleation. Homogeneous nucleation happens exclusively with substrates free from impurities. It occurs spontaneously through supercooling which can be described as cooling a liquid or gas far below its freezing point without solidification. In terms of water, the freezing point is generally considered to be 273.15 K equivalent to 0° C whereas crystal homogeneous nucleation can reach 224.8 K equivalent to −48.35° C through supercooling. Heterogeneous nucleation, however, occurs from an external interference in which the particles inside the liquid act as nucleation sites. In the case of heterogeneous nucleation it is more difficult to estimate measurements since the contact angle between particle and nucleus as well as the geometrical shape of the foreign particle should be considered [3].

1.1.2 Non-Photochemical Laser-Induced Nucleation

Non-photochemical laser-induced nucleation (NPLIN) was first hypothesised and introduced by a discovery in the mid 1990s by Garetz et al. [5]. The knowledge of the mechanism of the laser is still insufficient [3]. However, a recent paper, The Mechanisms of Non-Photochemical Laser-Induced Nucleation: Theory and Experiment written by T van

Waas, present four established theories including an interaction of molecular polarisation with the electric field and respective cavitation bubble formation by nanoparticle heating through light absorption [6]. Previous research papers have declared NPLIN to be a viable method of inducing nucleation [3].

1.1.3 Estimation of Velocity

The droplets have an inherent frequency before interacting with the laser beam and the actual frequency can be calculated using Equation (2) in which f_{drop} is drop frequency, Q is flow rate, V_{drop} is volume of droplets, and lastly D_{drop} is the diameter of the droplets.

$$f_{drop} = \frac{Q}{V_{drop}} = \frac{Q}{4\pi/3(D_{drop}/2)^3} \tag{2}$$

Moreover, in Equation (3) the velocity should be calculated in line with the droplet spacing to the adjacent neighbor, l_{drop}, and drop frequency, f_{drop} [1].

$$v = l_{drop} f_{drop} \tag{3}$$

1.1.4 Temperature Estimate

The Hertz-Knudsen theory of evaporation can be applied in order to find the temperature for when the actual nucleation takes place. Condensation and collisions are presupposed to be insignificant since the evaporation happens spontaneously. In this theory, the droplet is divided into 100 shells, as illustrated in Figure 2. Equation (4) presents the Hertz-Knudsen evaporation rate.

$$\gamma_e J_{e,max}(T_s) = \frac{(P_s(T_s) - P_v)}{\sqrt{2\pi m k_b T_s}} \tag{4}$$

The following Equation (5) calculates $\frac{dT_s}{dt}$ which is the surface temperature rate of the droplet through T_s that is temperature at the surface, t is time in ms and subsequently where $A_s(t)$ is the surface area of the evaporating droplet and $\rho(T_s)$ is the density. More-

over, $\frac{4\pi}{3}(r_{100}^3 - r_{99}^3)$ is the volume between surface of the droplet and adjacent inner-shell, r denotes the shell radius, $\Delta H_{vap}(T_s)$ is the enthalpy of evaporation and ultimately $C_p(T_s)$ is the specific heat capacity at constant pressure [7, 8].

$$\frac{dT_s}{dt} = -\gamma_e J_{e,max}(T_s) \frac{A_s(t)\Delta H_{vap}(T_s)}{\frac{4\pi}{3}(r_{100}^3 - r_{99}^3)\rho}(T_s) C_p(T_s) \tag{5}$$

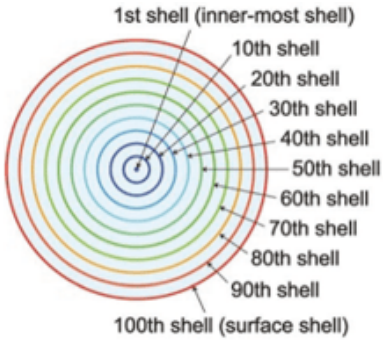

Figure 2: The Hertz-Knudsen theory of evaporation shells.

1.1.5 Nucleation Rate

The estimation of the ice nucleation rate J is based on the Classical Nucleation Theory, CNT. In Equation (6) the t stands for the time of the droplet's flight through the velocity and position, n and $n+1$ are two successive points in time and subsequently $f_{ice}(t_n)$ is the ice fraction at time n.

$$J(t_{n+1/2}) = -\frac{\frac{\ln[1-f_{ice}(t_{n+1}))}{(1-f_{ice}(t_n))]}}{V_{drop} \cdot (t_{n+1} - t_n)} \tag{6}$$

1.2 Aim of the Study

The aim was to, despite the stochastic nature of nucleation, implement temporal control of a homogeneous nucleation in supercooled water by introducing a laser pulse, and additionally spatial control through the shape and size of the laser beam spot. Ultimately, the aim was to find a lower threshold of power during laser-induced nucleation and comparing to laser-off, i.e. spontaneous nucleation [3].

2 Method

Initially the experimental setup of the mentioned NPLIN technique was interpreted thoroughly. This was followed by an explanation of data analysis and respectively calculations of that data. An estimate calculation of error was subsequently described and at last a methodology of the technique NPLIN utilized for this study.

2.1 Experimental Setup

A water container with 99 percent Milli-Q water, i.e. purified water through resin filters and deionization, allowed for a steady flow and was first processed by a water purification system with 18.2 MΩ.cm resistivity at ambient temperature. This water was subsequently compressed into tubes with ultrapure N_2 gas with 99.999 % and gas regulators to control the liquid flow. The water was pressurized through a reservoir and released into the chamber in the interest of excluding excess particles. Moreover, liquid nitrogen was applied under the vacuum chamber in order to supercool the chamber in advance of the droplets.

A nozzle inside the chamber produced droplets and comprised a glass orifice of 10 μm. A piezoelectric actuator inside the nozzle, that is able to record a diameter of 15 to 25 μm, recorded the size and spacing between the droplets. The diameter of the first droplet and spacing between was measured by utilizing an image processing package Fiji, as seen in Figure 3.

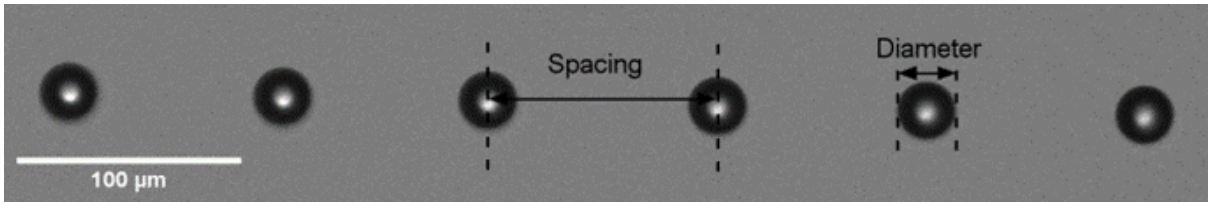

Figure 3: Image of the droplets released from the nozzle.

Furthermore, a flow meter was attached over the nozzle and two inline filters, maintaining fluid purity, with pore sizes of 90 an 0.5 μm between the reservoir and the nozzle. Changing the gas pressure provided a range of possible droplet velocities. A stable droplet

array with equal spacing was achieved through tuning the drop frequencies, tuning them together with the flow rate, in order to attain the condition able to estimate the speed and temperature.

A Q-switched Nd:YAG laser, titled Brilliant B, Quantel of 532 nm, illuminated the droplet array. This laser was synchronized with a camera CMOS, i.e. an image sensor based on a metal–oxide–semiconductor, camera titled FLIR Blackfly S, with a resolution of 2048 $\times$ 1536 pixels thus the camera was taking a picture every time the laser was sending a pulse generating real-time imaging. Additionally a fluorescent sheet was used in the laser path to make the pulse discrepant from the illumination that lights up the sample in the glass window of the chamber. An objective lens, 10$\times$ Mitutoyo Plan Apo Infinity corrected lens with a 30 mm working distance and an NA=0.28, was located inside the vacuum simultaneously as a tube lens, i.e. that minimizes the chromatic aberration by focusing red and blue light in the same point, behind the window port, Plano-convex lens f=200 mm, maintained focus of the collimated rays from the objective. The tube lens and the camera outside of the vacuum had a distance of 200 mm. In order to filter out the blue short wave-length incoming light there was also a long pass filter, specifically Longpass Filter of 550 nm, in front of the camera. Moreover, calibration was done through a 1951 USAF resolution test target of a microscopic camera had a resolution of 0.346 m/pixel.

In addition to the optics, steel shielding also directed the laser beam to the nozzle. Ultimately, Pharos, of 1030 nm and 1mj, an infrared laser, triggered the nucleation inside the droplets hit by the laser beam.

2.2 Data Analysis of Images and Calculations

The results of the laser induced nucleation were noted with particular regards to energy (µJ), power (W) and laser frequency (kHz) of the beam. Another column was used for the laser-off nucleation. Later the pictures were arranged, as seen in appendix A, with real time imaging by one droplet in every picture. This data was subsequently analysed and categorized into focused frames and unfocused droplets were omitted. The focused images

were thereafter arranged into liquid and frozen droplets, in line with the classification of Figure 4. This data was recorded and an ice fraction was calculated.

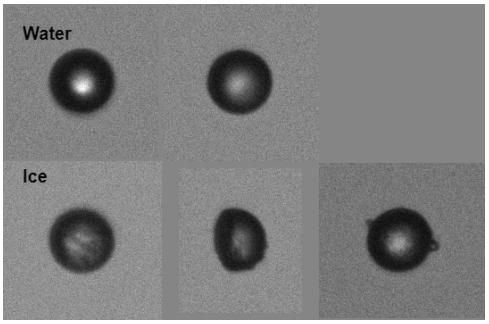

Figure 4: Image classification of water droplets and ice crystals after nucleation.

Moreover, the calculations of velocity, temperature, time and nucleation rate were preceded, as seen through code in appendix A.

2.2.1 Estimation of Error

The error estimates were numerically estimated through Monte Carlo simulations, see code in Appendix A, i.e. a mathematical simulation model that distributes probability of an uncertain occurrence. The binomial proportion confidence interval with 95% confidence was used and specifically The Wilson score interval which is asymmetric on the contrary, compared to the binomial interval [9].

2.3 Methodology

Conventional techniques are for instance suspending water droplets in oil, acoustic levitation of the droplets and droplets freezing on substrates that have been utilized in previous research. Nonetheless, homogeneous nucleation by supercooling the liquid far below its freezing point has a stochastic nature as regards to these methods due to the result being microscopic images and the impossibility to know the exact moment of the nucleation. Furthermore, these techniques also imply contact with a container wall thus increasing the risk of foreign particles and heterogeneous nucleation. Remote and external perturbations such as mechanical shock, electric fields or laser are therefore advantageous. Laser

induced nucleation offers the possibility to find time, location and morphology and does not preform any photo-chemical damage to the system [3]. NPLIN is also sustainable considering its energy sufficiency in comparison to traditional crystallization methods [6].

3 Results

The following results cover conditions of laser-induced respective laser-off nucleation. At first, an overview of constant values, subsequently tables of varying values and ultimately graphs illustrating the results. It should also be taken to account that the exact values of nucleation rates are submitted in code in Appendix A.

3.1 Laser-Induced Nucleation

The experiment with laser-induced nucleation had constant properties of a distance of 50 mm, flow rate Q 68,5 $^{-1}$, diameter D_{drop} 25.4 μm, spacing l_{drop} 94.8 μm and velocity v 12.614 ms^{-1}. Furthermore the time was 0.00396 s and temperature 233.386 K.

Table 1: Conditions of laser-induced nucleation regarding distance, total of focused and ice fraction.

Distance [mm]	**Total of focused droplets**	**Ice fraction** [%]
50	25	0
50	43	4.651
50	90	3.333
50	45	6.667
50	23	4.3

Table 2: Conditions of laser-induced nucleation regarding laser frequency, power and energy.

Laser frequency [kHz]	**Power** [W]	**Energy** [μj]
200	3	15
1000	3	3
1000	5	5
1000	7	7
1000	10	10

Table 3: Conditions of laser-induced nucleation regarding Wilson limit.

Distance [mm]	**Wilson lower limit** [%]	**Wilson higher limit** [%]
50	0	13.320
50	1.285	15.456
50	1.140	9.347
50	2.293	17.857
50	0.772	20.992

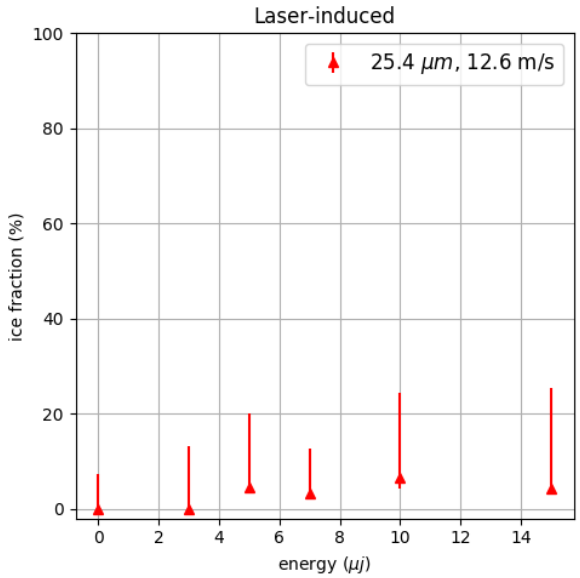

Figure 5: Laser induced graph presenting ice fraction relative to energy according to Table 1 and Table 2 where the vertical red lines expose Wilson score interval.

The focal point of the laser-induced nucleation should be the absence of a clear linear development in the graph Figure 5. However the Wilson bars overlaps and generally have an extensive Wilson higher limit.

3.2 Laser-off nucleation

The experiment with laser-induced nucleation had constant properties of a flow rate Q 68,5 μl/min, diameter D_{drop} 25.7 μm, spacing l_{drop} 95.7 μm and ultimately velocity v 12.293 m/s.

Table 4: Conditions of laser-off nucleation regarding distance, total of focused and ice fraction.

Distance [mm]	**Total of focused**	**Ice fraction** [%]
10	351	0
20	151	0
30	141	0
35	109	0.917
40	78	1.282
45	80	1.250
50	48	0
55	425	2.353
60	48	25

Table 5: Conditions of laser-off nucleation regarding distance, temperature and time.

Distance [mm]	**Temperature** T [K]	**Time** t [ms]
10	252.512	1
20	243.334	1.6
30	238.572	2.4
35	236.889	2.9
40	235.488	3.3
45	234.294	3.7
50	233.260	4.1
55	232.350	4.5
60	231.540	4.9

Table 6: Conditions of laser-off nucleation regarding Wilson limit.

Distance [mm]	**Wilson lower limit** [%]	**Wilson higher limit** [%]
10	0	1.083
20	0	2.481
30	0	2.65
35	0.162	5.015
40	0.227	6.911
45	0.221	6.746
50	0	7.410
55	1.283	4.277
60	14.920	38.785

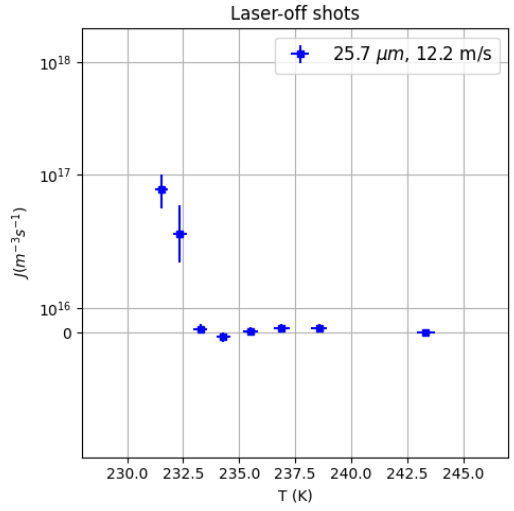

(a) Graph presenting nucleation rate, J, relative to temperature in line with Table 4 and Table 5.

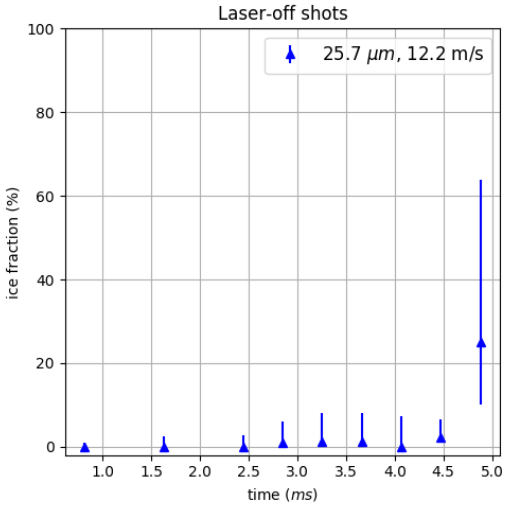

(b) Graph presenting icefraction relative to time in line with Table 4 and Table 5.

Figure 6: Laser-off graphs with vertical blue lines that expose Wilson score interval.

The focal point of the spontaneous nucleation is that the graph in Figure 6a indicates that the droplets started to nucleate at a temperature of 232 K and a negative nucleation rate at 233.260 K. The graph in Figure 6b expose that the ice fraction at 4.9 ms was 25%.

4 Discussion

As mentioned in the results section in the graph, Figure 5, the Wilson error bars overlaps. Despite of the higher energy responding to the highest ice fraction, the ice fractions do not correlate according to a steady linear development which indicates that higher energy of the laser beam did not provide a larger steady percentage of ice fraction. Additionally a considerable difference between energies would indicate when the laser would impact the nucleation which is not visible in the graph. Therefore simply a upper threshold of power, 10 W, for future research is obtained and no temporal or spatial control implemented.

Figure 6a implicates that the droplets started to nucleate at a temperature of 232 K since a considerable difference in nucleation rates was observed. It also suggest a negative nucleation rate at approximately 233.260 K.

Figure 6b illustrates that within 4.9 ms there were 25% fully frozen droplets. It is essential to address that 0 % ice fraction at 50 mm and a negative nucleation rate do not align with the conventional theory of freezing homogeneous liquid or the laser-induced nucleation and thus poses a dilemma. The negative nucleation rates are due to the low statistics around some of the measured points and thus are not accurate. The ideal nucleation rate should always be higher as the droplets get colder. Sufficiently number of shots need to be collected in order to avoid poor statistics and consequently, these unexpected decrease in the nucleation rates. Additionally, the Wilson distribution at 4.9 ms is extensive thus minimizing the accuracy.

4.1 Further research

The method used for these experiments can be improved in further research. For instance utilizing an infrared camera ensuring the laser beam to be directed precisely to the nozzle and higher power, thus optimistically implementing control. Furthermore the deviant dilemma of the 0 % ice fraction at 50 mm can be improved through increasing number of attempts since unfocused images were disregarded as well as the small number of images at 50 mm which was 48 compared to previous, as seen in Table 4 .

Granting an extraordinary spatial and temporal control as well as identifying a lower threshold of power will allow us to investigate nucleation mechanisms. Since laser-induction is triggered remotely, phase diagrams can therefore also be developed. It is for instance possible to detect new polymorphs that can be used in active pharmaceutical ingredients as well as atmospheric science and thus climate change. Further research in this field will ultimately be momentous.

4.2 Conclusion

Since a linear development or a considerable difference of the laser-induced nucleation was not visible, the conclusion is that the laser was not able to induce the nucleation, delivering the presented boundaries. Further research can therefore utilize this experiment study's upper threshold for power, 10 W as a lower threshold for laser induced nucleation . However it is vital to take improvements of the method into account such as, for instance, the accuracy in the direction of the laser, pointing an infrared camera, into the chamber.

References

[1] Sosso GC, Chen J, Cox SJ, Fitzner M, Pedevilla P, Zen A, et al. Crystal nucleation in liquids: Open questions and future challenges in molecular dynamics simulations. Chemical reviews. 2016;116(12):7078–7116.

[2] Murray B, O'sullivan D, Atkinson J, Webb M. Ice nucleation by particles immersed in supercooled cloud droplets. Chemical Society Reviews. 2012;41(19):6519–6554.

[3] Alexander AJ, Camp PJ. Non-photochemical laser-induced nucleation. The Journal of chemical physics. 2019;150(4):040901.

[4] Debenedetti PG. Metastable liquids. Princeton university press; 2021.

[5] Garetz B, Aber J, Goddard N, Young R, Myerson A. Nonphotochemical, polarization-dependent, laser-induced nucleation in supersaturated aqueous urea solutions. Physical review letters. 1996;77(16):3475.

[6] van Waas T. The Mechanisms of Non-Photochemical Laser-Induced Nucleation: Theory and Experiment. 2019.

[7] Knudsen M. Die maximale verdampfungsgeschwindigkeit des quecksilbers. Annalen der Physik. 1915;352(13):697–708.

[8] Hertz H. Ueber die Verdunstung der Flüssigkeiten, insbesondere des Quecksilbers, im luftleeren Raume. Annalen der Physik. 1882;253(10):177–193.

[9] Vallejo A, Muniesa A, Ferreira C, de Blas I. New method to estimate the sample size for calculation of a proportion assuming binomial distribution. Research in veterinary science. 2013;95(2):405–409.

A Code

The code used in the method as well as in results can be found at: https://github.com/soremilia/Rays/blob/main/Rays_summerschool2021-main%20(1).zip